PHYSICAL REVIEW B VOLUME 52, NUMBER 11 15 SEPTEMBER 1995-I

# Optical-phonon Raman-scattering study of short-period GaAs-AlAs superlattices: An examination of interface disorder

G. S. Spencer and J. Menéndez
*Department of Physics and Astronomy, Arizona State University, Tempe, Arizona 85287-1504*

L. N. Pfeiffer and K. W. West
*AT&T Bell Laboratories, Murray Hill, New Jersey 07974*

(Received 13 March 1995)

The effect of cation intermixing on the Raman spectrum of GaAs-AlAs superlattices has been investigated. Experimental measurements are compared with theoretical predictions based on fully three-dimensional supercell calculations. The accuracy of the modeled Raman spectra makes it possible to evaluate different mechanisms of interface disorder on a quantitative basis. In particular, a detailed comparison is made between the compositional profiles predicted by gallium-surface-segregation models and those resulting from simple cation intermixing at the GaAs-AlAs interfaces. Best agreement with experiment is obtained for the predictions of the surface-segregation models. These models, however, are unable to account simultaneously for the growth temperature dependence of the GaAs-like and AlAs-like Raman spectra, even when the kinetics of the disordering process is fully taken into account.

## I. INTRODUCTION

The development of epitaxial-growth techniques has opened an entirely new field in semiconductor physics. Two-dimensional electron gases with striking properties, strained-layer systems, and quantum-well devices are just a few in a long list of new developments during the past 15 years.[1] The basic building block of these structures, i.e., the interface between differing materials, has received considerable attention. Early photoluminescence (PL) experiments on high-quality GaAs-$Al_xGa_{1-x}As$ quantum-well systems showed a splitting of the main emission line into several closely spaced peaks.[2–4] The energy separating these peaks was found to correspond to well thickness fluctuations of 1 or 2 ML. These results were interpreted in terms of atomically flat islands of size at least as large as the Bohr radius of the exciton. Subsequent high-resolution transmission electron diffraction (HRTEM) experiments, however, failed to observe these large, atomically flat islands.[5,6] In fact, considerable cation intermixing was detected in the interface layers, and this intermixing was observed to occur over several monolayers. The microscopy data are consistent with more recent optical and Raman-scattering experiments.[7–9] The present consensus is that the interface disorder has a bimodal character, comprised of a short-range component and a long-range component.[7] The short-range component is the cation intermixing on the atomic scale observed in the HRTEM experiments. The long-range component results in the large island structure observed by the PL experiments.

Although a consensus appears to have been reached as to the structure of the superlattice interface, the actual disordering mechanism is much less clear. Surface segregation of gallium atoms has recently been suggested as a source of interface roughness for materials grown by molecular-beam epitaxy (MBE).[7–13] The tendency for gallium to segregate to the surface during the epitaxial growth of $Al_xGa_{1-x}As$ alloys is well documented.[10,11,14–16] This process is, therefore, a primary candidate for the explanation of the short-range, atomic-scale component of the interface roughness. Since surface segregation appears to be intrinsic to the epitaxial-growth process, this implies that atomically perfect GaAs-AlAs structures cannot be fabricated using MBE.

An important feature of the surface-segregation process in GaAs-AlAs structures is the long-range penetration of the gallium atoms into the AlAs layers. This penetration is consistent with Raman-scattering experiments, which suggest that the cation intermixing is not limited to the layers closest to the interface. On the other hand, the Raman data suggest a dramatic improvement in the structural perfection of the interface as the MBE growth temperature is reduced from about $T_g = 500\,^{\circ}C$ to $T_g = 400\,^{\circ}C$ and below. This temperature dependence is not accounted for by simple segregation models using experimental activation energies.[13] It has been suggested that the temperature dependence arises from kinetic limitations to the segregation process.[13,17] To our knowledge, however, no attempt has been made to correlate the Raman spectra in superlattices with the predictions from kinetically limited segregation models.

In this paper, we present an in-depth Raman study of interface disorder in GaAs-AlAs superlattices. Our experimental data are compared with very accurate supercell calculations of the Raman spectra, which make it possible to assess the validity of different models of interface disorder. In particular, we consider in detail the gallium-surface-segregation predictions, including the case of kinetically limited segregation. Our modeling

0163-1829/95/52(11)/8205(14)/$06.00  

shows very clearly that the surface-segregation idea provides a better overall explanation of the Raman spectra than any other model where the cation intermixing is limited to the layers closest to the interfaces. On the other hand, we find very significant deviations between experiment and the predictions from the surface-segregation model, not only in the growth temperature dependence of the Raman spectra, as reported earlier,[12] but also in the fact that the surface-segregation model is unable to account simultaneously for the GaAs- and AlAs-like Raman spectra of our superlattices. This leads to the conclusion that a one-dimensional picture of surface segregation, where the gallium atoms segregate to ideally flat surfaces, is incorrect. Instead, our results are consistent with a recent suggestion by Braun and Ploog that segregation takes place preferentially at surface steps.[18]

Our experimental data suggest that the surface-segregation model works best for samples grown at temperatures near $T_g = 450\,^{\circ}\mathrm{C}$. Deviations from the model predictions become dramatic for GaAs-AlAs superlattices grown at $T_g = 350\,^{\circ}\mathrm{C}$, for which we find that the GaAs layers are essentially perfect while the AlAs layers show clear evidence for the presence of gallium. Measurements of the GaAs-like $E_0$ electronic transition in these samples are in excellent agreement with calculated transition energies for perfect superlattices. These encouraging results indicate that gallium segregation may not be the ultimate limit to structural perfection in GaAs-AlAs superlattices grown at low temperatures. For growth at high temperature ($T_g = 600\,^{\circ}\mathrm{C}$) we also find large deviations from the predictions of the surface-segregation model. The Raman peaks observed from these samples cannot be assigned to the standard series of confined phonon modes, suggesting a very complicated layer intermixing pattern, possibly with spatial inhomogeneities.

Since the structural conclusions drawn from our data are based on our ability to model the Raman spectra of our superlattices, it is critically important to access the validity and limitations of this method. Raman scattering has long been recognized as a powerful tool in the investigation of the structural perfection of the GaAs-AlAs interface.[19–24] The expected Raman spectrum for atomically perfect single layers and superlattices can be easily computed, and the discrepancies observed with experiment are a most sensitive indicator of structural imperfections. Raman spectroscopy has significant advantages over other optical techniques, such as PL or absorption spectroscopy, because the phonon structure is much easier to compute than the electronic structure. On the other hand, while the probe size for optical techniques (including Raman spectroscopy) is of the order of micrometers or more, the effective spatial resolution in a Raman experiment is much better when the Raman-active vibrations are localized over atomic-size regions. This is the case for GaAs-AlAs superlattices, where GaAs- and AlAs-like vibrations are localized in their respective layers. Previous Raman work has confirmed the inequivalence of the direct (AlAs on GaAs) and inverted (GaAs on AlAs) interfaces,[7] has provided definitive proof for the presence of gallium in all "AlAs" layers of the superlattice when the total "AlAs" region thickness is 4 ML or less,[13,25,26] and has given evidence for the validity of the surface-segregation model in the explanation of interface disorder in these structures.[13]

While the sensitivity of Raman scattering to interface disorder is very dramatic, the possibility of extracting quantitative structural information is limited by a number of factors, which we will address in this paper. Ideally, we would like to *fit* the experimental Raman spectrum with a theoretical expression where the only adjustable function is the cation distribution. This involves the calculation of the frequencies and intensities of different Raman modes. For disorder to be included exactly in the calculation of Raman spectra, large atomic supercells are necessary. Supercell calculations, however, are computationally intensive. Attempts have been made to use approximate methods to include disorder effects,[27–31] but these methods suffer from the limitation that the basic physics behind disorder-induced frequency shifts is three-dimensional and microscopic in nature. In the case of optical phonons in GaAs-AlAs superlattices, there are two fundamental physical effects that require supercell treatment. First, the curvature of the phonon branches depends on the crystalline direction. In perfect (001) superlattices only the (001) direction matters, but when disorder is present all directions become important. Second, a gallium atom in a nominal AlAs layer or an aluminum atom in a nominal GaAs layer does not participate in optic-mode vibrations. This leads to a reduction of the dynamical effective charge and a corresponding reduction of the longitudinal-transverse-optic-mode splitting. This decrease has been shown to be the main cause of the frequency shift observed for the AlAs-like optic phonons in disordered GaAs-AlAs superlattices[26] and $Al_xGa_{1-x}As$ alloys.[32]

For the calculation of phonon frequencies with the accuracy required by the Raman experiments, only first-principles calculations yield suitable results. This type of calculation, however, is not practical for large supercells with hundreds of atoms. Fortunately, recent first-principles calculations of bulk-phonon dispersion relations show that the interatomic force constants are similar for most tetrahedral semiconductors and virtually identical for GaAs and AlAs.[33] The similarity of the GaAs and AlAs force constants has recently been confirmed by second-order Raman-scattering studies on AlAs.[34,35] In addition, more recent studies have shown that the similarities of GaAs and AlAs also extend into third-order terms in the expansion of the crystal potential.[36] Since the force constants of GaAs and AlAs are essentially the same, one does not expect them to change when the superlattice is formed. In fact, first-principles calculations of superlattice phonons confirm that the use of bulk interatomic force constants is perfectly adequate[33,37] and hence a fully self-consistent calculation is not needed. This result makes it possible to use large supercells for the calculation of phonons in disordered superlattice systems and $Al_xGa_{1-x}As$ alloys, without sacrificing the accuracy of first-principles methods.[26] In this paper we use a full three-dimensional model to calculate phonons in disordered GaAs-AlAs superlattices.

This model takes advantage of the similarity of the GaAs and AlAs force constants[33] and effective charges[34] by treating the disordered superlattices as a mass perturbation of the bulk material.[38]

While the frequencies and eigenvectors of phonons in disordered GaAs-AlAs superlattices can be calculated from very accurate *ab initio* methods, there is no practical first-principles approach to the determination of Raman intensities. A calculation of the scattered light intensity involves integrations over excited electronic states the energy of which cannot be computed correctly within the local-density approximation. Thus, aside from the enormous computational complications of such calculations, the introduction of empirical or adjustable parameters is unavoidable.[39,40] In the limit where the laser photon energy is much smaller than the lowest electronic transition, the Raman tensor can be written as a sum of bond-polarizability derivatives.[41] The corresponding Raman intensities can be easily computed in terms of the phonon eigenvectors and a few polarizability parameters that characterize the Ga-As and Al-As bonds. These parameters can be fit to bulk Raman data. Unfortunately, bond-polarizability models are expected to break down as the laser photon energy approaches optical transition energies and the Raman intensity becomes resonantly enhanced.[40] This is particularly so for Raman scattering induced by the Fröhlich electron-phonon interaction. It is customary in this field to denote spectra obtained utilizing $Ar^+$ excitation ($E_L \sim 2.3-2.5$ eV) as "off resonance." This denomination is useful in distinguishing these spectra from those recorded for excitation at energies in extreme resonance with the lowest excitonic transition. Off-resonance Raman spectra are frequently analyzed in terms of bond-polarizability models. However, since the laser photon is well within the absorption range of the structure, the conditions for the validity of these models are not fulfilled. Only in those cases where the resonance enhancement is similar for all models involved should one expect a detailed agreement between calculated and experimental line shapes.

In addition to the breakdown of the bond-polarizability approach, an important phenomenon observed in the resonant regime is the violation of wave-vector conservation. For superlattices, this has dramatic consequences due to the angular dependence of the polar optic modes.[42] In particular, the so-called "interface modes"[43] are nothing but the angular-dependent phonons made Raman active by a breakdown of wave-vector conservation. It is customarily assumed that these effects become important only near extreme resonance, but we will show in this paper that they are also significant for off-resonance spectra.

Since the predicted Raman peak positions depend mainly on the force constants used, our tests of compositional profiles based on these frequencies are expected to be very accurate. On the other hand, our predicted Raman line shapes are based upon the bond-polarizability model and the assumption of wave-vector conservation within the supercell picture. Hence the information on compositional profiles provided by these line shapes is more qualitative.

## II. THEORY

In order to model the effects of disorder on the superlattice Raman spectra, we have computed the phonon dynamics using the approach of Chang, Ren, and Chu.[38] The superlattice-mode displacements $\{\mathbf{u}_j\}$ are expressed in terms of the bulk-solution basis $\{\mathbf{u}_g^{(0)}\}$,

$$\mathbf{u}_j = \sum_g A_{jg}\mathbf{u}_g^{(0)} , \tag{1}$$

where the indices $j$ and $g$ label the superlattice and bulk modes, respectively. In this manner, the superlattice equations of motion yield the generalized eigenvalue problem[44]

$$\omega_j^2(\mathbf{k})\{M^{\mathrm{SL}}\mathbf{I}+\underline{\Delta\mathbf{M}}^{\mathrm{SL}}\}\,\mathbf{A}_j = \{M^{\mathrm{SL}}\underline{[\omega^{(0)}(\mathbf{k})]^2}+\underline{\Delta\mathbf{D}}^{\mathrm{SL}}\}\,\mathbf{A}_j , \tag{2}$$

where $\omega_j$ is the superlattice-model frequency and $M^{\mathrm{SL}}$ is the total mass of the superlattice cell. The matrices $\underline{\Delta\mathbf{M}}^{\mathrm{SL}}$ and $\underline{\Delta\mathbf{D}}^{\mathrm{SL}}$ are the change in mass and dynamical matrix from the bulk problem in the basis of the bulk problem. The matrix $\underline{[\omega^{(0)}(\mathbf{k})]^2}$ is the diagonal matrix of bulk eigenvalues. The use of Eq. (2) is motivated by the first-principles result $\underline{\Delta\mathbf{D}}^{\mathrm{SL}} \to 0$ for GaAs-AlAs superlattices.[33] In particular, the similarity of the effective changes means that the direct computation of the Coulomb matrix elements can be bypassed completely. This is advantageous, because, in low-dimensional structures such as superlattices, the determination of the Coulomb matrix elements is a tedious task and requires the use of a generalized Ewald transformation method.[45] With $\underline{\Delta\mathbf{D}}^{\mathrm{SL}} \to 0$, Eq. (2) is reduced to a mass-perturbation problem.

The similarity of the GaAs and AlAs force constants is a first-principles result. However, due to the lack of published first-principles force constants, we utilize a rigid-ion model in the calculation of our bulk eigenvalues and eigenvectors.[46] In order to minimize the effects of using the rigid-ion model, we use model parameters that have been fit to the dispersion relations of Giannozzi *et al.*[33] in a manner which optimizes the optic-mode dispersions. The parameters used are given in Table I. We further reduce the effects of the rigid-ion model by using the GaAs bulk solutions as the unperturbed basis in the calculation of the GaAs-like modes and the AlAs bulk solutions for the AlAs-like modes.

Superlattice disorder is included by considering large supercells containing 792 atoms. These supercells consist of 12 cation and anion layers of 33 atoms. In this way, we are able to realistically model the $6\times6$ superlattices studied here with alloying in increments of 3% within each layer. We consider some simple models of interface disorder, namely, superlattices containing partially alloyed layers and superlattices with compositional profiles determined using McLean's segregation law, in which only the surface and the first underlying layer interact.[47] Thus the surface and bulk compositions are linked by[47]

$$\ln\left[\frac{x_{\mathrm{Al}}^s}{1-x_{\mathrm{Al}}^s}\right]+\chi=\ln\left[\frac{x_{\mathrm{Al}}^b}{1-x_{\mathrm{Al}}^b}\right] , \tag{3}$$

TABLE I. The rigid-ion model parameters used in this study are tabulated. These parameters have been fit to the first-principles calculations of Giannozzi *et al.* (Ref. 33) in a manner which optimizes the optical-branch dispersions.

| Material | $A$ | $B$ | $C_1$ | $D_1$ | $E_1$ | $F_1$ | $C_2$ | $D_2$ | $E_2$ | $F_2$ | $q$ |
|---|---|---|---|---|---|---|---|---|---|---|---|
| GaAs | −0.416 | −0.1861 | −0.28 | +0.046 | +0.089 | −0.093 | −0.050 | −0.113 | +0.07 | +0.20 | 0.626 |
| AlAs | −0.413 | −0.1664 | −0.0435 | −0.006 | +0.010 | +0.0213 | −0.0185 | −0.080 | +0.05 | +0.156 | 0.716 |

where $x^i_{\mathrm{Al}}$ is the fraction of aluminum in a layer and the indices $s$ and $b$ represent the surface and first-underlying layers, respectively. The parameter $\chi$ is defined as $\chi \equiv E_S/k_bT_g$, where $k_b$ is the Boltzmann constant. We use a phenomenological segregation energy of $E_S=0.10$ eV (energy liberated when a gallium atom in the underlying layer displaces an aluminum surface-layer atom).[10] One such superlattice profile is shown in Fig. 1. The dashed lines represent the profile for a perfect superlattice. The apparent shift of the "GaAs" and "AlAs" regions is due to the gallium segregation. The fraction of aluminum present in each layer of the superlattice profile is then rounded to the nearest 3% to fit the 33 atom/layer basis. Using these "segregation profiles," the superlattice atoms are randomly distributed within each layer and the superlattice phonons are calculated.

Equation (3) is the thermodynamic limit where the system has infinite time to complete the atomic exchanges in the two outermost surface layers. Under real growth conditions, however, there is a finite time for these processes, which is determined by the growth rate of the structure. In such cases, a kinetic model may be needed to simulate the segregation process. In a recent letter, Dehaese, Wallart, and Mollot[17] demonstrated the kinetic nature of indium segregation in the $In_{1-x}Ga_xAs$ system using the kinetic model of exchange processes.[48–50] We have followed the approach of Dehaese, Wallart, and Mollot to generate kinetically limited segregation profiles. In the kinetic model, the segregation of gallium (indium in the case of Ref. 17) from the bulk of the surface and from the surface to the bulk are described in terms of overcoming energy barriers. The energy barrier for a gallium atom's bulk-to-surface exchange $E_1$ differs from that of the surface-to-bulk exchange $E_2$ by the phenomenological segregation energy $E_S$ used in the McLean segregation law (see inset of Fig. 2). If the segregation is assumed to be due only to the exchange process, then the rate of incoming and outgoing gallium surface atoms is given by[17]

$$\frac{dx^s_{\mathrm{Ga}}(t)}{dt}=\phi_{\mathrm{Ga}}+P_1x^b_{\mathrm{Ga}}(t)x^s_{\mathrm{Al}}(t)-P_2x^s_{\mathrm{Ga}}(t)x^b_{\mathrm{Al}}(t)\ , \tag{4}$$

where $\phi_{\mathrm{Ga}}$ is the gallium deposition rate in ML/sec and $x^i_{\mathrm{Ga}}(t)$ and $x^i_{\mathrm{Al}}(t)$ are the time-dependent surface or bulk gallium and aluminum concentrations, respectively. The exchange process is governed by overcoming the respective barriers at a rate $P_i(t)=\nu_i\exp(-E_i/k_bT_g)$, where $\nu_i$ is a typical vibrational frequency and is taken to be $10^{13}$ $s^{-1}$ for both exchange processes. The conservation of gallium atoms and the total number of surface atoms at any time $t$ lead to the conditions[17]

$$x^s_{\mathrm{Ga}}(t)+x^b_{\mathrm{Ga}}(t)=x^s_{\mathrm{Ga}}(0)+x^b_{\mathrm{Ga}}(0)+\phi_{\mathrm{Ga}}t \tag{5}$$

and

$$x^s_{\mathrm{Ga}}(t)+x^s_{\mathrm{Al}}(t)=x^s_{\mathrm{Ga}}(0)+x^s_{\mathrm{Al}}(0)+(\phi_{\mathrm{Ga}}+\phi_{\mathrm{Al}})t\ , \tag{6}$$

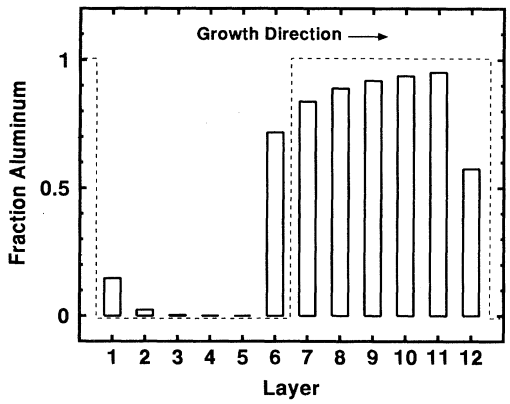


FIG. 1. A 6×6 superlattice segregation profile calculated using Eq. (3) is plotted. The parameters assumed are $E_S=0.10$ eV and $T_g=350$ °C (Ref. 7). The dashed line represents the profile of a perfect superlattice. The apparent shift of the superlattice profile is an effect of the segregation. Note the presence of a significant fraction of gallium atoms throughout the "AlAs" layers.

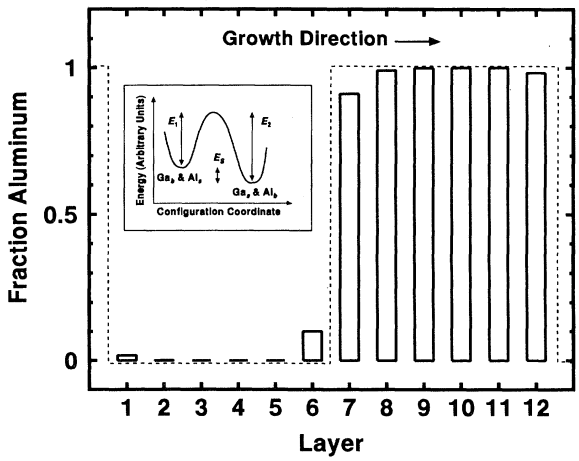


FIG. 2. A 6×6 superlattice kinetic-segregation profile calculated using Eqs. (4)–(6) is plotted. The inset shows the definition of the kinetic-segregation parameters. The parameters used in the determination of the profile shown are $E_1=1.7$ and $E_2=1.8$ eV with $T_g=350$ °C. The dashed line represents the profile of a perfect superlattice.

respectively. The segregational profile can be determined by numerically solving Eqs. (4)–(6). A kinetic-segregation profile for $T_g = 350\,^{\circ}\mathrm{C}$ is shown in Fig. 2.

In the manner described above, we are able to realistically model the lattice dynamics of disordered superlattices using a fully three-dimensional treatment. The bond-polarizability model is then used to describe the electron-phonon interaction in the determination of the Raman intensities from the atomic displacements.[51] It should again be noted that the bond-polarizability model assumes the system to be in a nonresonant excitation condition. Although excitation "away" from *extreme* resonance is typically termed "off resonance," it is an experimental necessity to work in the away-from-extreme-but-still-close-to-resonance condition. Clearly, the largest limitation to this treatment of disordered superlattices is the determination of the Raman intensity from the lattice dynamics using the bond-polarizability model. Therefore, one cannot expect the calculated Raman spectra to exactly fit the experimental Raman intensities.[40]

## III. EXPERIMENT

We studied $(GaAs)_6(AlAs)_6$ (6×6) superlattices grown by MBE on undoped (001) GaAs substrates using a modified GEN II MBE system.[52] The samples were grown at a substrate temperature $T_g$ of 350, 450, or 650 °C. A total of 160 superlattice periods were deposited at a rate of 1 Å/sec without interruptions on a 3000-Å-thick GaAs buffer layer grown on (100) substrates (not intentionally misoriented) at a temperature of 650 °C. The Raman experiments were performed at room temperature using discrete $Ar^+$ and $Kr^+$ laser lines and tunable dye lasers. The light was scattered off the superlattice's (001) face in the $z(x,y)\bar{z}$ and $z(x,x)\bar{z}$ configurations [incident wave vector along $z$, scattered wave vector along $\bar{z}$, incident polarization along $x$, and scattered polarization along $x$ or $y$ with $x=(100)$, $y=(010)$, and $z=(001)$]. The scattered light was dispersed by a SPEX 1404 double monochromator and detected with either a SPEX CCD charge-coupled device optical multichannel analyzer or a photomultiplier tube.

## IV. RESULTS

### A. Sample characterization

#### 1. $E_0$ transitions

Although we try to avoid extreme resonance when attempting to model the disordered superlattice Raman spectra, the excitation profiles near extreme resonance contain useful information about the superlattice characteristics. The peak of the Raman excitation profile corresponds to the $E_0$ transition. The resonant excitation Raman profiles for the $LO_2$ modes of the three superlattice samples are given in Fig. 3. The peak of the resonance profiles has been shown to correspond to the outgoing channel.[43,53] Therefore, the optical transition $E_0$ for the superlattice can be determined using

$$E_0 = E_L - \hbar\omega_p \ , \tag{7}$$

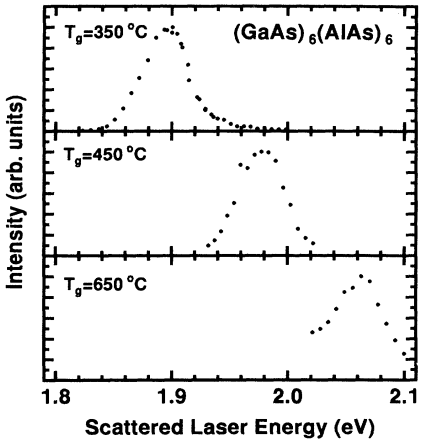


FIG. 3. The experimental resonant Raman excitation profile of the $LO_2$ phonon is plotted for the three superlattice samples. The resulting band gaps are tabulated in Table II. Note the increasing band gap with increasing superlattice growth temperature.

where $E_L$ is the energy at which the resonance Raman profile peaks, $\omega_p$ is the frequency of the phonon, and we neglect excitonic effects on the energy (excitonic energies $\approx 5$ meV, much less than the width of the resonance). The experimental optical transition energies $E_0$ for the three samples are tabulated in Table II. Clearly, $E_0$ is observed to increase with increasing superlattice growth temperature. In order to provide a reference with which to compare the transition energies of these samples, we estimate the $E_0$ transition energy for a perfect 6×6 superlattice. Zhang and co-workers have calculated the $E_0$ transition in $(GaAs)_n(AlAs)_n$ superlattices using first-principles self-energy corrections to the local-density approximation.[54,55] They predict for a $(GaAs)_6(AlAs)_6$ superlattice an $E_0$ transition 350 meV below the $E_0$ transition of a virtual-crystal alloy defined as the arithmetic average of the corresponding transitions in GaAs and AlAs. Using the experimental $E_0$ values for GaAs and AlAs, we obtain for our $(GaAs)_6(AlAs)_6$ superlattice $E_0 = 1.87$ eV.[56] This shows excellent agreement with the value for the $T_g = 350\,^{\circ}\mathrm{C}$ superlattice, whereas the higher-temperature superlattices have a higher $E_0$. The implications of these results may be interpreted using the simple, one-dimensional particle-in-a-box problem. In this problem, as the width of the well decreases, the energy of the well modes increase. Therefore, the $E_0$ results suggest a distortion of the square well shape as the superlattice growth temperature is increased. The good agreement between theory and the experimental results for the $T_g = 350\,^{\circ}\mathrm{C}$ sample suggests that this sample is much closer to perfection. We will show that this is consistent with the experimental Raman peak positions.

#### 2. Acoustic phonons

In a GaAs-AlAs superlattice, the periodicity of the structure manifests itself in a "folding" of the bulk-material acoustic modes. This causes the appearance of

TABLE II. The experimental $E_0$ transition energy and acoustic doublet peak positions for the three superlattice samples are tabulated. Also listed are the theoretical predictions for these properties in a perfect 6×6 superlattice. Note the excellent agreement of the $T_g=350$ °C sample's values with the perfect superlattice predictions.

| Superlattice type | | $E_0$ | First acoustic doublet positions | |
|---|---|---|---|---|
| Experiment | | | | |
| | $T_g=350$ °C | 1.87 eV | 47.3 $cm^{-1}$ | 50.9 $cm^{-1}$ |
| | $T_g=450$ °C | 1.95 eV | 49.8 $cm^{-1}$ | 53.7 $cm^{-1}$ |
| | $T_g=650$ °C | 2.03 eV | 52.8 $cm^{-1}$ | 56.8 $cm^{-1}$ |
| Theory | Perfect superlattice | 1.87 eV | 48.2±1.1 $cm^{-1}$ | 51.8±1.1 $cm^{-1}$ |

acoustic doublets in the superlattice Raman spectrum. The room-temperature Raman spectra of the first-acoustic doublet for the three superlattice samples are shown in Fig. 4. These spectra were taken at the resonant energies determined from Fig. 3. The peak positions, adjusted for direct comparison with low-temperature theory, are tabulated in Table II. These acoustic-phonon frequencies may be used to verify sample periodicity, and, in conjunction with AlAs-like interface modes, the effective period of the superlattice layers.[43] These measurements are analogous to the periodicity measurements obtainable from x-ray scattering. Note that as the superlattice growth temperature is increased, the acoustic doublets shift to a higher energy.

The positions of the acoustic doublet calculated for a perfect 6×6 superlattice are also given in Table II. While the doublet for the $T_g=350$ °C sample is in good agreement with the theoretically predicted values for a perfect superlattice, the $T_g=450$ and 650 °C samples exhibit increasingly higher-energy doublets with somewhat larger splitting. These doublets suggest a shorter effective period, for the higher-temperature samples, of up to 1 ML for the $T_g=650$ °C sample. Comparison of the Raman peak frequencies of the AlAs-like interface modes indicates that the GaAs and AlAs layers have the same thickness in the $T_g=350$ °C sample, whereas in the $T_g=650$ °C sample a larger fraction of the missing monolayer must originate in the GaAs layers.[43]

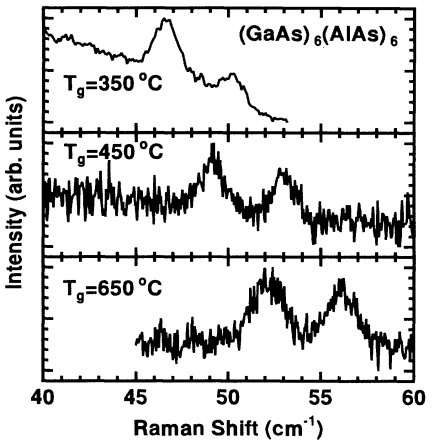


FIG. 4. The experimental Raman spectra of the first acoustic doublets for the three superlattice samples is plotted. Note the increasing phonon energy with increasing superlattice growth temperature. The doublet positions are tabulated in Table II.

### B. Modeling of the off-resonance Raman intensity using the bond-polarizability model

#### 1. Experimental results

The Raman spectra of 6×6 superlattices grown at the three different temperatures are shown in Figs. 5 and 6 as thick solid lines. The scattering configuration is $z(x,y)\bar{z}$. For bulk GaAs and AlAs, only one Raman peak at 290 or 403 $cm^{-1}$, respectively, is observed in this configuration. This peak corresponds to the long-wavelength ($q\approx 0$) longitudinal-optic (LO) phonon. In a $(GaAs)_n(AlAs)_n$ superlattice, with $2(n+n)$ atoms per

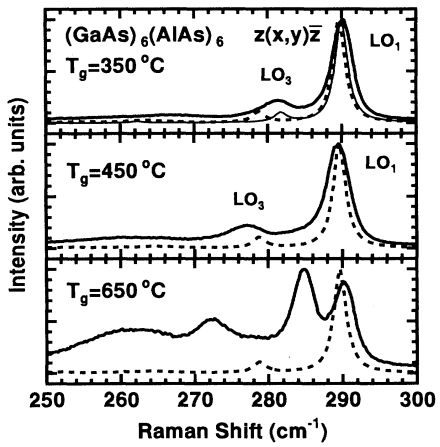


FIG. 5. The experimental Raman spectra (thick solid lines) of the GaAs-like optic modes in $(GaAs)_6(AlAs)_6$ superlattices are plotted for three different superlattices growth temperatures. The scattering configuration is $z(x,y)\bar{z}$ using $Ar^+$ excitation of $E_L=2.41$ eV. Note that as the growth temperature is increased, the optic modes shift to lower energy. For a discussion of the appearance of new peaks in the $T_g=650$ °C spectra, see text. The theoretical segregation-disordered GaAs-like Raman spectra (dashed line) calculated using the mass-perturbed-bulk model are also plotted. The segregation profiles are determined using $E_S=0.10$ eV. The thin solid line is the calculated Raman spectrum for a perfect superlattice. Notice that the $T_g=350$ °C superlattice experimental results are fit well by the theoretical *perfect* superlattice. The optic-mode peak positions are tabulated in Table III.

unit cell, there are $n+n$ LO phonon branches. The displacement eigenvectors corresponding to $n$ of the Raman-active phonons from these branches are localized in the GaAs layers (GaAs-like modes), while the other $n$ LO phonons are localized in the AlAs layers (AlAs-like modes). These modes are referred to as "confined" LO phonons and are labeled $LO_j$ ($1 \leq j \leq n$), where the count starts at the highest-energy mode in each layer.[41] Modes with $j$ odd are Raman allowed in the $z(x,y)\bar{z}$ configuration. Modes with $j$ even are Raman allowed in the $z(x,x)\bar{z}$ configuration but their intensity is very weak except near extreme resonance, where they are enhanced by the Fröhlich interaction.[41] The phonon confinement is due to the elastic mismatch between GaAs and AlAs, which manifests itself in the well-separated bulk optic-mode energies. Figure 5 shows the GaAs-like $LO_j$ Raman modes and Fig. 6 the AlAs-like modes. A summary of peak positions is given in Table III.

In determining the peak positions in Table III, several corrections have been made. The experimental peak positions are taken from Lorentzian fits to the room-temperature data, and corrected using neon emission lines as a standard. The calculated superlattice GaAs- and AlAs-like mode energies are shifted such that the calculated energies of bulk GaAs and AlAs, respectively, agree with those obtained experimentally at room temperature. (The experimental bulk positions are also corrected by neon emission lines.) In this manner, direct comparison of the experimental and theoretical peak po-

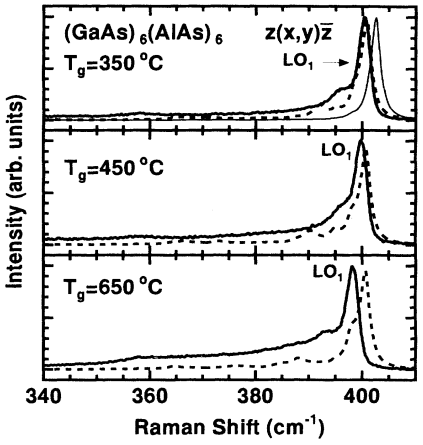


FIG. 6. The experimental Raman spectra (thick solid line) of the AlAs-like optic modes in $(GaAs)_6(AlAs)_6$ superlattices are plotted for three different superlattice growth temperatures. The scattering configuration is $z(x,y)\bar{z}$ using $Ar^+$ excitation of $E_L=2.41$ eV. Note the shift to lower energies of the high-energy optic-mode peak as the superlattice growth temperature is increased. The theoretical segregation-disordered AlAs-like Raman spectra (dashed line) calculated using the mass-perturbed-bulk model are also plotted. The segregation profiles are determined using $E_S=0.10$ eV. The thin solid line is the calculated Raman spectrum for a perfect superlattice. The optic-mode peak positions are tabulated in Table III.

TABLE III. The experimental longitudinal-optic phonon peak positions for the GaAs- and AlAs-like modes in 6×6 superlattice Raman spectra in Figs. 5 and 6 are tabulated. The $LO_2$ mode positions are obtained from spectra taken in the $z(x,x)\bar{z}$ configuration. The theoretical calculations are for segregation profiles determined by Eq. (3) using the values of $\chi \equiv E_S/k_bT_g$ specified (Ref. 7). The growth temperatures corresponding to $E_S=0.10$ eV are indicated by parentheses. The calculated Raman spectra for a perfect superlattice as well as the $T_g=350$, 450, and 650 °C profiles are plotted with the experimental data in Figs. 5 and 6. The phonon energies are given in $cm^{-1}$. An asterisk denotes that peak positions for the $T_g=650$ °C sample do not correspond to $LO_i$ as indicated. Due to the uncertainty in peak assignment, the highest-energy GaAs-like peak is tabulated under $LO_1$, the next highest under $LO_2$, and so forth. These positions are given for comparison with the lower-growth-temperature superlattice peak positions.

| | | GaAs-like | | | | AlAs-like |
|---|---|---|---|---|---|---|
| | Superlattice type | $LO_1$ | $LO_2$ | $LO_3$ | $LO_1$-$LO_3$ | LO |
| Experiment | | | | | | |
| | $T_g=350$ °C | 290.1 | 286.6 | 281.2 | 8.9 | 400.8 |
| | $T_g=450$ °C | 289.4 | 283.7 | 277.4 | 12.0 | 400.2 |
| | $T_g=650$ °C | 290.3* | 284.8* | 279.3* | 11.0* | 398.3* |
| Theory | | | | | | |
| | Perfect superlattice | 289.9 | 287.0 | 281.7 | 8.2 | 402.6 |
| $\chi=3.59$ | ($T_g=50$ °C) | 289.6 | 285.8 | 279.7 | 9.9 | 401.5 |
| $\chi=2.74$ | ($T_g=150$ °C) | 289.5 | 285.5 | 279.0 | 10.6 | 401.0 |
| $\chi=2.22$ | ($T_g=250$ °C) | 289.4 | 285.2 | 278.6 | 10.8 | 400.8 |
| $\chi=1.86$ | ($T_g=350$ °C) | 289.2 | 284.8 | 278.5 | 10.7 | 400.9 |
| $\chi=1.61$ | ($T_g=450$ °C) | 289.2 | 284.8 | 278.2 | 11.0 | 400.7 |
| $\chi=1.41$ | ($T_g=550$ °C) | 289.2 | 284.7 | 278.3 | 10.9 | 400.8 |
| $\chi=1.26$ | ($T_g=650$ °C) | 289.1 | 284.4 | 278.1 | 11.0 | 400.5 |

sitions can be made. Another effect which can change the experimental absolute peak position is the mismatch strain between GaAs and AlAs. Although GaAs and AlAs are nearly lattice matched, the AlAs layers are slightly strained to accommodate the lattice constant of the GaAs substrate. Assuming the anharmonic parameters describing the effect of the strain on AlAs vibrations to be constant throughout the Brillouin zone, we obtain an additional shift in the AlAs-like mode energies of $-1.0$ cm$^{-1}$.[57] The effect of the strain shift is minimized by obtaining the bulk AlAs Raman spectra using unrelaxed epitaxial AlAs grown on a GaAs substrate. However, the mode Grüneisen parameter is known to change near the zone edge, and therefore the shift due to strain is dependent upon mode energy. This effect, though, is neglected because it is expected to cause only a small change in the $-1$-cm$^{-1}$ strain shift found above.

### 2. *Predictions for perfect superlattices and comparison with experiment*

The predicted Raman spectra for perfect $6\times6$ superlattices, using a bond-polarizability model, are shown as the thin solid lines in the top panels of Figs. 5 and 6. In both cases, the calculated spectrum has been normalized to the intensity of the strongest peak and given the same Lorentzian broadening found experimentally in bulk measurements. For the $z(x,y)\bar{z}$ configuration, the $LO_1$, $LO_3$, and $LO_5$ modes are Raman active.[41] Experimentally, only the $LO_1$ and $LO_3$ peaks can be identified unambiugously. Their intensity ratio is in good agreement with the theoretical prediction. The fact that the $LO_5$ peak is not observed is also consistent with the very weak intensity predicted for this Raman mode at 262 cm$^{-1}$. It is apparent that the bond-polarizability model gives a reasonable account of the relative intensities of the GaAs-like Raman peaks, in spite of the fact that the conditions for its validity are not fulfilled. This is because the relative intensity of these peaks depend mainly on the eigenvectors of the corresponding phonons[58] and not on resonance effects.

The large separation between individual $LO_j$ peaks in the GaAs-like superlattice Raman spectrum is a result of the downward curvature of the bulk GaAs LO dispersion relation. On the other hand, the bulk AlAs LO dispersion along the (001) direction is very flat.[33] This leads to very small confinement downshifts for the AlAs-like $LO_j$ phonons in a superlattice structure. Hence the expected AlAs-like Raman spectrum features a single, broadened peak at a frequency very close to that of bulk AlAs.

Several significant deviations between experiment and the predicted Raman spectra for a perfect $6\times6$ superlattice can be observed in Figs. 5 and 6, and Table III.

(i) As the growth temperature is increased, the GaAs-like $LO_1$ and $LO_3$ phonons shift to lower energy, and the $LO_1$-$LO_3$ splitting increases.

(ii) In the $T_g=650\,^{\circ}$C sample, GaAs-like Raman peaks are observed which cannot be indexed as even- or odd-index $LO_j$ modes.

(iii) The experimental AlAs-like $LO_1$ peak is considerably downshifted from its predicted position.

(iv) A less intense second peak at 395 cm$^{-1}$ and a broad mesalike structure down to 360 cm$^{-1}$ are observed in the AlAs-like spectra for all samples.

These deviations contain valuable structural information about the interface. In order to extract this information, we have investigated the effect on the Raman spectrum of several models of interface disorder. These models are described in the following sections. Some conclusions, however, can be drawn without any further modeling, as pointed out in previous work.[7,25,26] In particular, the downshift of the AlAs-like $LO_1$ peak cannot be understood without the presence of gallium in the nominally pure AlAs layers. The (001) phonon modes in a perfect superlattice grown along the (001) direction can be written as linear combinations of (001) bulk phonons. Since the dispersion of these modes is very small in AlAs, no significant frequency downshift is obtained. However, the presence of gallium in these layers mixes in bulk phonons propagating in other directions, for which the dispersion is significant.[33] This can induce a larger downshift of the superlattice AlAs-like modes. In addition, alloying reduces the LO-TO splitting, causing a further decrease of the mode frequency.[32] It is important to reemphasize here that these effects, unlike confinement shifts, cannot be adequately treated with one-dimensional dynamic models.

### 3. *Dual interfacial alloying*

A simple model that is frequently invoked to explain the Raman spectra of GaAs-AlAs superlattices is a random alloying occurring at both superlattice interfaces. Comparisons have been made between the experimental GaAs-like peak positions and calculations using one-dimensional[9] and three-dimensional[26] models. Using our three-dimensional model, we have calculated the GaAs- and AlAs-like peak positions in $(GaAs)_6(AlAs)_6$ superlattices for random alloying at both interfaces. The depth of alloying is taken to be 1 or 2 ML. (Note that 1 ML intermixing is taken to mean 1 ML on each side of the interface, yielding a 2-ML-wide alloy region.) In Fig. 7 the GaAs- and AlAs-like peak positions are plotted as a function of alloy layer composition. In the case of the 2 ML alloying, the central alloy layers are taken to be $Al_{0.5}Ga_{0.5}As$. (See top panels of Fig. 7.) The solid (dashed) lines in the figure represent the $T_g=350\,^{\circ}$C ($T_g=450\,^{\circ}$C) experimental peak positions. Note that while the GaAs-like peak positions can be reproduced using the dual-alloying mechanism, as has been shown previously,[12] the significant downshift of the AlAs-like $LO_1$ mode cannot be simultaneously predicted for either of the superlattice growth temperatures. This is because the central "AlAs" layers are gallium-free within this model. Due to the flat (001) LO-phonon dispersion in AlAs, the frequency of a slab as thin as 2 ML is much higher than the value experimentally observed for a layer with a nominal thickness of 6 ML. This disordering scheme is also unable to predict the additional structure observed in the $T_g=650\,^{\circ}$C GaAs-like spectra of Fig. 5.

In addition to the lack of quantitative agreement between the AlAs-like experimental results and theory, extreme qualitative differences are observed. This is shown in Fig. 8 where the calculated Raman spectrum for a dual-interfacial-alloying superlattice and a thermodynamic-limit segregation-disordered superlattice are plotted along with the experimental data for the $T_g = 450\,^{\circ}\mathrm{C}$ sample. The dual-interfacial-alloy predictions show a significant modal structure in the energy range of the AlAs-like mesa structure. This additional structure corresponds to modes which are localized in the interfacial-alloy regions of the superlattice.[26] The combination of the lack of quantitative and qualitative agreement between theory and experiment implies that the simple dual-random-interfacial-alloying mechanism is insufficient to model the superlattice disorder observed.

Figure 7 shows that the GaAs-like modes of the $T_g = 350\,^{\circ}\mathrm{C}$ sample are in excellent agreement with the

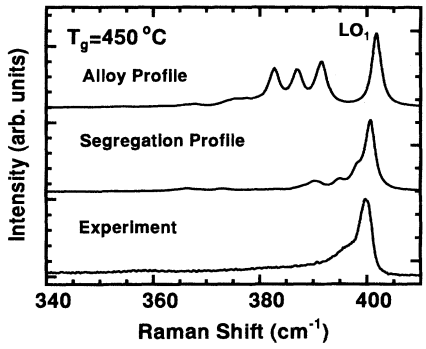


FIG. 8. The experimental AlAs-like $z(x,y)\bar{z}$ Raman spectra for $T_g = 450\,^{\circ}\mathrm{C}$ is plotted along with the dual-interfacial-alloying and segregation-model predictions. The alloy calculation is for 50% alloying on the first interface layer and 30% on the second. Notice the presence of several additional peaks in the low-energy AlAs-like region.

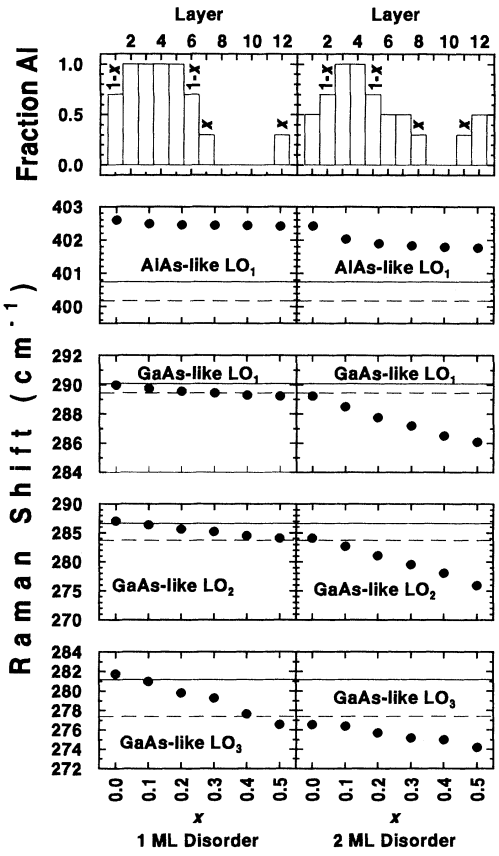


FIG. 7. The calculated GaAs- and AlAs-like peak positions are plotted vs alloy composition for $(GaAs)_6(AlAs)_6$ superlattices with random alloying at both interfaces. 1-ML alloying implies alloying within 1 ML of the interface, yielding a 2-ML alloy region. Note that for alloying greater than 1 ML, the central layers are taken to be $Al_{0.5}Ga_{0.5}As$. The compositional profiles are shown in the top panels of the figure. The solid (dashed) lines represent the experimental results for the $T_g = 350\,^{\circ}\mathrm{C}$ ($T_g = 450\,^{\circ}\mathrm{C}$) sample. Note the inability to simultaneously predict the GaAs- and AlAs-like positions.

predictions for a *perfect* superlattice. The observation of $E_0$ transitions at about the energy predicted for perfect superlattices indicates that the lateral dimensions of these nearly perfect GaAs layers is at least of the order of 100 Å. This is consistent with simulations of the Raman spectrum. These simulations require lateral dimensions of the order of hundreds of Å in order to observe Raman peaks near the predictions for perfect layers. On the other hand, the AlAs-like Raman spectrum of the same sample deviates strongly from the prediction for a perfect superlattice, indicating the presence of gallium in the nominally AlAs layers.

### 4. *Alloying at a single interface*

From the point of view of the growth process, there are two different interfaces in the GaAs-AlAs superlattice structure: the direct interface (AlAs deposited on GaAs) and the inverted interface (GaAs deposited on AlAs). The inequivalence of these interfaces has been demonstrated using Raman spectroscopy by Jusserand *et al.*[7] As a possible way to simulate the effects of this inequivalence on superlattice disorder, we have calculated the superlattice phonon peak positions assuming a 1-, 2-, or 3-ML random alloying at only one interface. The calculated GaAs- and AlAs-like peak positions as a function of alloy composition are plotted in Fig. 9. In the case of the 2- and 3-ML intermixing the central alloy layers are taken to have an $Al_{0.5}Ga_{0.5}As$ composition. The solid (dashed) line represents the experimental results for the $T_g = 350\,^{\circ}\mathrm{C}$ ($T_g = 450\,^{\circ}\mathrm{C}$) sample. Note that the results are similar to those for the dual-interfacial-alloying case in Fig. 7. However, in the single-asymmetric-alloying case the discrepancies between theory and experiment are even greater, requiring more cation intermixing per layer in order to achieve the necessary downshifts in the GaAs-like modes. As in the dual-interfacial-alloying scheme, the additional structure observed in the $T_g = 650\,^{\circ}\mathrm{C}$ GaAs-like spectrum, as well as the significant downshift of the AlAs-like $LO_1$ mode, is not predicted.

### 5. *Superlattice modeling of segregation-induced disorder*

The Raman spectra for the thermodynamic-limit segregation profiles obtained using Eq. (3) with $E_S=0.1$ eV and $T_g=350$, 450, and 650 °C are plotted, along with the experimental data, as the dashed lines in Figs. 5 and 6. The corresponding GaAs- and AlAs-like peak positions are tabulated in Table III and are displayed graphically in Fig. 10. Notice that the model calculations for the disordered superlattices show some qualitative similarity to the experimental results. Clearly, as the growth temperature increases we are able to reproduce the downward shift AlAs-like $LO_1$, GaAs-like $LO_1$, and $LO_3$; the increase of the $LO_1$-$LO_3$ splitting; and the presence of the AlAs-like low-energy optic mode. Examination of the calculated mode displacement pattern for the AlAs-like low-energy optic mode shows it to have a distorted $LO_3$ pattern, confirming the one-dimensional model results of Jusserand and Mollot.[13] This distortion causes the mode to have a more $LO_1$-like displacement pattern, thus increasing its intensity with respect to the $LO_3$ mode in a perfect superlattice. In addition to these features, some of the AlAs-like "mesa" structure is predicted in Fig. 6. However, the structure of the calculated Raman spectra in the AlAs-like "mesa" region still tends to be modal (peaked), and not mesalike as found by experiment.

Taking a more quantitative look at the experimental and theoretical results (see Table III and Fig. 10), we see that the $T_g=450$ °C sample's peak positions are closest to the segregation-model predictions for both the GaAs- and AlAs-like modes. However, samples grown at both lower and higher temperatures are not in as good agreement. In the case of the $T_g=350$ °C sample we find that the AlAs-like $LO_1$ peak position is correctly predicted using the segregation model. At the same time, the GaAs-like peak positions are closer to those of a *nearly perfect* $6\times6$ superlattice ($\chi\rightarrow\infty$). As is the case with the previously discussed alloy disordering schemes, the segregation model is unable to explain the additional modes that appear in the GaAs-like spectrum for the $T_g=650$ °C sample in Fig. 5.

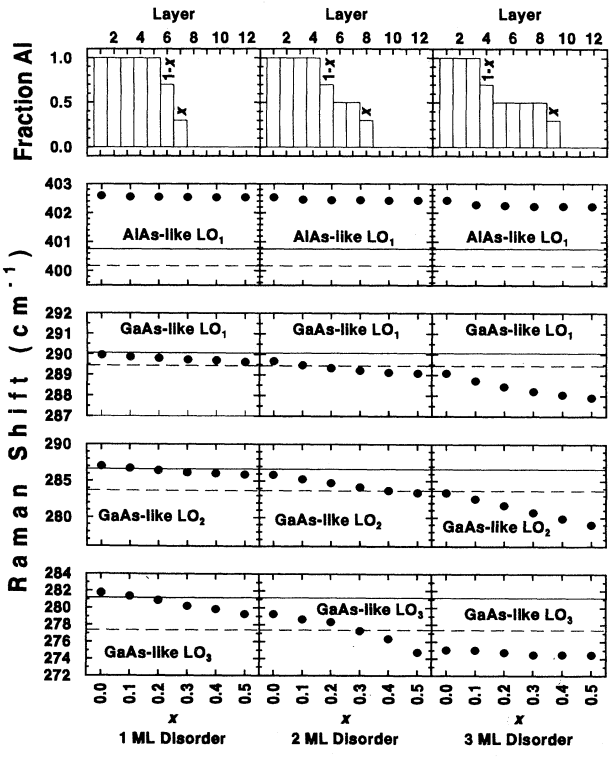


FIG. 9. Same as Fig. 7 with alloying at only one interface. This simulates the effect of the asymmetric superlattice composition caused by the inequivalence of the direct and inverted interface. Clearly this asymmetry *alone* cannot account for the observed interface disorder.

### 6. *Kinetically limited segregation*

Since the thermodynamic segregation model of the preceding section is unable to simultaneously explain the GaAs- and AlAs-like experimental results in the $T_g=350$

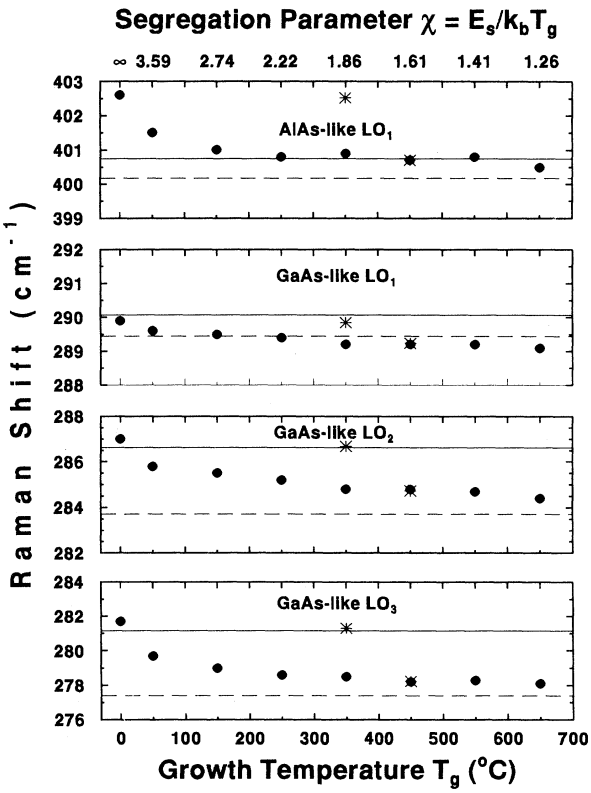


FIG. 10. The calculated GaAs- and AlAs-like segregation-disordered superlattice peak positions are plotted linearly vs growth temperature. The McLean segregation profiles are for a segregation energy of $E_S=0.10$ eV (solid circles). The segregation parameter $\chi$ corresponding to each temperature is plotted on the top axis. The solid (dashed) lines represent the experimental results for the $T_g=350$ °C ($T_g=450$ °C) sample. Note the inability to simultaneously model the near-perfect nature of the $T_g=350$ °C sample's GaAs region while predicting the disordered nature of the AlAs region. The peak positions for a kinetic-segregation profile are also plotted (asterisks).

and 450 °C samples, we now calculate the Raman spectra for superlattices with kinetically limited segregation profiles. In the kinetic-segregation model, the value of the barrier energy is a key parameter for the evaluation of compositional profiles. Because the segregation process is not yet understood at the atomic level, there are no theoretical predictions as to the value of the barrier. As mentioned by Dehaese, Wallart, and Mollot,[17] it should be of the order of the binding energy of the atoms. Since we are trying to find out whether a kinetically limited process might explain the differences between the samples grown at $T_g=350$ and 450 °C, we have adopted a somewhat reversed procedure in that we look for reasonable values of the barrier that might explain the temperature dependence. For the barrier energies $E_1=1.7$ and $E_2=1.8$ eV, i.e., $E_S=0.1$ eV, with a 1-ML/sec superlattice growth rate, we find that virtually no segregation takes place for $T_g=350$ °C, while at $T_g=450$ °C the segregation is nearly identical to the McLean segregation profile. The calculated Raman peak positions for these kinetic-segregation disordered superlattice profiles are given by the asterisks in Fig. 10. Note that the peak positions for the $T_g=350$ °C profile are near those for a perfect superlattice while the $T_g=450$ °C positions match those of the McLean segregation model. However, while we now have good agreement between theory and experiment for the $T_g=350$ °C GaAs-like modes and the $T_g=450$ °C GaAs- and AlAs-like modes using the kinetic-segregation profiles, the $T_g=350$ °C AlAs-like modes are still in disagreement. Due to this qualitative deficiency of the model, which casts some doubt on its validity, we are unable to fit the barrier heights to the experimental data.

## V. DISCUSSION

### A. Segregation model accuracy

The simulations discussed in the previous paragraphs illustrate the limitations of the segregation models. Experimentally, when the growth temperature is decreased from $T_g=450$ to 350 °C one sees a dramatic change in the GaAs-like phonons and a small change in the AlAs-like phonons. The segregation model in its thermodynamic limit is able to account reasonably well for the AlAs-like phonons, but fails to explain the growth temperature dependence of the GaAs-like modes. This temperature dependence is accounted for by a kinetic-limited segregation process, but such a model wold also predict a comparable temperature dependence in the AlAs-like range. It is quite apparent that neither approach can explain the experimental data completely.

Recently, Braun and Ploog have proposed that the segregation of gallium atoms takes place preferentially at step edges.[18] The effect of the presence of a step on the segregation energy and barriers is not known; however, it is conceivable that it effectively lowers the segregation energy and/or barriers in such a way as to allow significant segregation to occur. In the exchange process, the gallium atom which segregates to the surface is replaced by an aluminum atom. Since this aluminum atom now resides in the bulk layer, its mobility should be small. Thus if the steps are widely spaced, large regions of the GaAs layers would appear to be pure. The gallium atom which segregated to the surface, on the other hand, would have a higher mobility. This could lead to a significant fraction of gallium atoms throughout the AlAs layers, thus causing a downshift of the AlAs-like $LO_1$ phonon while the GaAs-like Raman spectrum is dominated by the perfect regions. The size of the supercells needed to verify this scenario is beyond our present modeling capabilities. It is quite apparent from the existing data and simulations, however, that the simple one-dimensional kinetic-segregation model is not sufficient to characterize the disorder in the superlattice samples.

Since the McLean segregation law has been shown to be successful in the modeling of $Al_xGa_{1-x}As$ alloys,[14,15] its failure in the case of GaAs-AlAs superlattices seems somewhat surprising. This failure may be due to the difference in the nature of the alloy structure from that of the superlattice. The GaAs-AlAs superlattice is by definition a very ordered structure when compared to the random nature of the alloy. One might expect the abruptness of the superlattice interface to have a dramatic effect on the mechanism of gallium segregation. The simple segregation law used in this study is unable to take these differences into account, since this involves more than just the stoichiometry of the surface and first-underlying layer.

The limitations of the segregation model are also apparent for samples grown at higher temperatures. The experimental Raman data for the $T_g=650$ °C sample show large deviations from the segregation-model predictions. In addition to this sample we also performed experiments on a $T_g=620$ °C sample grown in the same manner. This sample revealed Raman spectra similar to that of the $T_g=650$ °C sample. Braun and Ploog have also found an anomaly in superlattices grown in this temperature range.[18] (This temperature range coincides with the "forbidden range" of $Al_xGa_{1-x}As$ growth where the surface morphology of the material degrades.)[59] They observed irregularities in the reflection high-energy electron-diffraction intensity oscillation shapes during growth. These irregularities are interpreted in terms of a GaAs surface-phase transition in the growth of samples at or above $T_g=633$ °C. A similar surface-phase transition is observed to occur for AlAs at or above $T_g=613$ °C. Raman spectroscopy is extremely useful when the broad characteristics of the compositional profiles are known. In the case of the high-growth-temperature samples, the possible structures leading to their complicated Raman spectra are probably too many to be modeled in a meaningful way without additional input from a direct imaging technique. This analysis is currently underway.

### B. Failure of the bond-polarizability model

Because our approach allows the calculation of the Raman spectrum for any given compositional profile, we are not limited to the predictions of the segregation model. In fact, we have calculated the Raman spectra for many alternative profiles. It is quite apparent from these calcu-

lations that some specific features of the Raman spectrum cannot be reproduced. The most significant is the mesalike structure found in the AlAs-like Raman spectra of Fig. 6. Insight into the origin of this structure is gained through the AlAs-like spectra in the $z(x,x)\bar{z}$, polarized configuration. The AlAs-like Raman spectra in the $z(x,x)\bar{z}$ configuration for the $T_g=350$, 450, and 650 °C samples are shown in Fig. 11. Notice that the mesalike structure is visible for all of these samples. The observation of the mesalike structure in both configurations and its strength in the polarized configuration suggest that it may be a forbidden process. As mentioned previously, the presence of disorder in the superlattice disturbs the symmetry of the lattice in such a way as to cause a weakening of wave-vector conservation. This weakening of the conservation rule leads to an effective "sampling" of the wave-vector orientation. Near extreme resonance this effect is dramatically enhanced due to double-resonance effects,[60] and leads to the so-called interface modes.

To simulate the breaking of wave-vector conservation, we have calculated the angular density of states for the GaAs- and AlAs-like modes in a perfect $6\times6$ superlattice using a random incident wave-vector orientation with magnitude determined by a Gaussian profile centered at $k=0$. The width of the Gaussian distribution is chosen equal to the incident-laser wave vector. The calculated angular density of states for the GaAs- and AlAs-like energy ranges are shown in Fig. 12. Notice that in the AlAs-like angular density of states a wide plateau ranging from 360 to 395 $cm^{-1}$ is observed. We propose that this plateau produces the mesalike structure in the AlAs-like Raman spectra of Fig. 6. The origin of this plateau is coupled to the nearly flat nature of the AlAs dispersion along the direction of superlattice growth.[33] This contributes a set of modes densely packed at about 400 $cm^{-1}$ to the density of states. In the region from about 365 to 395

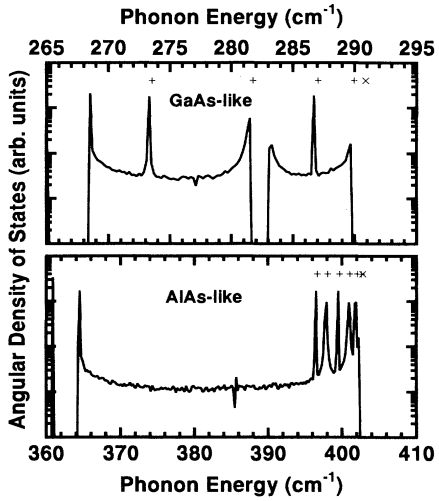


FIG. 12. The angular density of states for the GaAs- and AlAs-like optic modes in a perfect superlattice are plotted. The "+" symbols represent the position of the Γ-point superlattice $LO_i$ phonons while the "×" symbols represent that of the bulk material. Note the dispersed and condensed nature of the GaAs- and AlAs-like $LO_i$ modes, respectively. The broad tableau nature of the AlAs-like angular density of state in the range 360–395 $cm^{-1}$ may be the source of the mesalike feature exhibited in Fig. 6.

$cm^{-1}$ the angular dispersions of the TO and LO modes are nearly linear, have no anticrossings like those observed around 400 $cm^{-1}$, and intersect for in-plane wave vectors. This leads to a nearly constant contribution to the angular density of states. The angular density of states in Fig. 12 is, thus, the combination of this nearly constant plateau and the clustered peaks.

In the case of GaAs, on the other hand, the LO dispersion in the (001) direction is curved downward, leading to

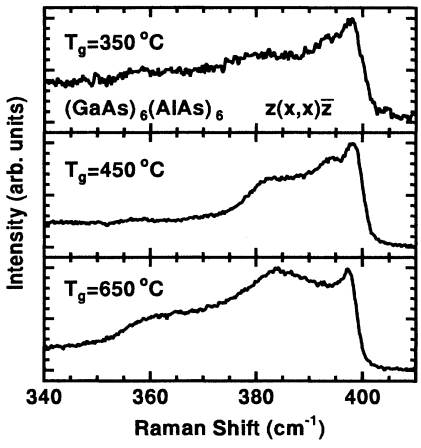


FIG. 11. The experimental Raman spectra of the AlAs-like optic modes in $(GaAs)_6(AlAs)_6$ superlattices are plotted for three different growth temperatures. The scattering configuration is $z(x,x)\bar{z}$ using $Ar^+$ excitation of $E_L=2.41$ eV. Note that the mesalike structure observed in Fig. 6 is also observed here.

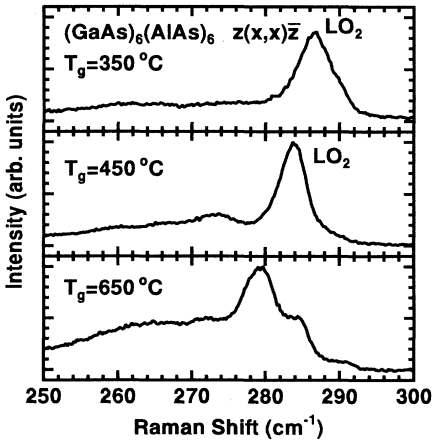


FIG. 13. The experimental Raman spectra of the GaAs-like optic modes in $(GaAs)_6(AlAs)_6$ superlattices are plotted for three different growth temperatures. The scattering configuration is $z(x,x)\bar{z}$ using $Ar^+$ excitation of $E_L=2.41$ eV. Note the structure observed in addition to the superlattice even-index $LO_i$ modes expected in this configuration.

well-separated modes and a peaked angular density of states. The angular density of states for the GaAs-like modes is plotted in Fig. 12. The gap in the angular density of states observed near 280 $cm^{-1}$ is due to the anticrossing of the $LO_1$ and $LO_3$ modes in the angular dispersion.[61] This anticrossing leads to two well-separated structures in the angular density of states. However, it is difficult to discern these features in the $z(x,y)\bar{z}$ configuration spectra of Fig. 5 due to the widely dispersed nature of the LO modes. In Fig. 13 we give the GaAs-like Raman spectra for the $T_g = 350$, 450, and 650 °C samples in the $z(x,x)\bar{z}$ configuration where the Fröhlich interaction effects are strongest. Clearly, there is structure observed in these spectra that is not attributable to the superlattice even-index LO modes expected in this configuration.[41]

## VI. CONCLUSIONS

We have conducted Raman-scattering studies of the effects of gallium-surface-segregation in GaAs-AlAs superlattices. Our study features a very accurate three-dimensional calculation of superlattice vibrations, which makes it possible to draw quantitative conclusions as to the validity of different models of interface disorder. We have found that current surface-segregation models are unable to account for all the features of the Raman spectra. In particular, the ability of these models to simultaneously explain the GaAs- and AlAs-like Raman data indicates that the cation compositional profiles are not one dimensional. Thus a realistic model of interface disorder must take into account the morphology of the growing surface, including the presence of steps that may affect the efficiency of the surface-segregation process.[18]

Modeling of the Raman spectrum of disordered superlattices requires accurate phonon energies and Raman intensities. Our results suggest that a bond-polarizability model, while not strictly valid for laser excitation in the visible-energy range, is reasonably good for GaAs-AlAs superlattice calculations because the relative intensities of the different phonon peaks are mainly determined by the corresponding displacement eigenvectors. However, we observe clear resonance-effect deviations from the bond-polarizability model predictions that make it difficult to fit the Raman spectrum to a given compositional profile. In particular, the broad mesalike structure always observed in the AlAs-like Raman spectrum is assigned to a density-of-states feature induced by a breakdown of wave-vector conservation.

## ACKNOWLEDGMENTS

We would like to express our appreciation to John Page for providing the code with which the Coulomb matrix elements used in this study are calculated, as well as to acknowledge the fruitful discussions on the determination of Coulomb matrix element effects in semiconducting materials. This work has been supported by the National Science Foundation under Grant No. DMR-88-14918, DMR 90-58343, and DMR 91-21567.

[1]For a review, see E. O. Göbel and K. Ploog, Prog. Quantum Electron. **14**, 289 (1990).
[2]L. Goldstein, Y. Horikoshi, S. Tarucha, and H. Okamoto, Jpn. J. Appl. Phys. **22**, 1489 (1983).
[3]B. Deveaud, J. Y. Emery, A. Chomette, B. Lambert, and M. Baudet, Appl. Phys. Lett. **45**, 1078 (1984).
[4]R. F. Kopf, E. F. Schubert, T. D. Harris, and R. S. Backer, Appl. Phys. Lett. **58**, 631 (1991).
[5]A. Ourmazd, D. W. Taylor, J. Cunningham, and C. W. Tu, Phys. Rev. Lett. **62**, 933 (1989).
[6]A. Ourmazd, F. Baumann, M. Bode, and Y. Kim, Ultramicroscopy **34**, 237 (1990).
[7]B. Jusserand, F. Mollot, J.-M. Moison, and G. Le Roux, Appl. Phys. Lett. **57**, 560 (1990).
[8]C. A. Warwick, W. Y. Jan, A. Ourmazd, and T. D. Harris, Appl. Phys. Lett. **56**, 2666 (1990).
[9]D. Gammon, B. V. Shanabrook, and D. S. Katzer, Phys. Rev. Lett. **67**, 1547 (1991).
[10]J. M. Moison, C. Guille, F. Houzay, F. Barthe, and M. Van Rompay, Phys. Rev. B **40**, 6149 (1989).
[11]J. M. Moison, F. Houzay, F. Bathe, J. M. Gérard, B. Jusserand, J. Massies, and F. S. Turco-Sandroff, J. Cryst. Growth **111**, 141 (1991).
[12]B. Jusserand, F. Mollot, R. Planel, E. Molinari, and S. Baroni, Surf. Sci. **267**, 171 (1992).
[13]B. Jusserand and F. Mollot, Appl. Phys. Lett. **61**, 423 (1992).
[14]T. C. Chiang, R. Ludeke, and D. E. Eastman, Phys. Rev. B **25**, 6518 (1982).
[15]J. Massies, F. Turco, A. Salettes, and J. P. Contour, J. Cryst. Growth **80**, 307 (1987).
[16]R. Kohleick, A. Förster, and H. Lüth, Phys. Rev. B **48**, 15 138 (1993).
[17]O. Dehaese, X. Wallart, and F. Mollot, Appl. Phys. Lett. **66**, 52 (1995).
[18]W. Braun and K. H. Ploog, J. Appl. Phys. **75**, 1993 (1994).
[19]J. Sapriel, J. C. Michel, J. C. Tolédano, R. Vacher, J. Kervarec, and A. Regreny, Phys. Rev. B **28**, 2007 (1983).
[20]K. Kubota, N. Nakayama, H. Kotah, and N. Sano, Solid State Commun. **49**, 157 (1984).
[21]M. V. Klein, C. Colvard, R. Fischer, and H. Morkoç, J. Phys. C **5**, 131 (1984).
[22]B. Jusserand, F. Alexandre, D. Paquet, and G. Le Roux, Appl. Phys. Lett. **47**, 301 (1985).
[23]D. Levi, Shu-Lin Zhang, M. V. Klein, J. Klem, and H. Morkoç, Phys. Rev. B **36**, 8032 (1987).
[24]G. Fasol, M. Tanaka, H. Sakaki, and Y. Horikoshi, Phys. Rev. B **38**, 6056 (1988).
[25]J. Grant, J. Menédez, L. N. Pfeiffer, K. W. West, E. Molinari, and S. Baroni, Appl. Phys. Lett. **59**, 2859 (1991).
[26]E. Molinari, S. Baroni, P. Giannozzi, and S. de Gironcoli, Phys. Rev. B **45**, 4280 (1992).
[27]M. Bernasconi, L. Colombo, and L. Miglio, Phys. Rev. B **43**, 14 457 (1991).
[28]D. Kechrakos, P. B. Briddon, and J. C. Inkson, Phys. Rev. B **44**, 9114 (1991).
[29]B. Samson, T. Dumelov, A. A. Hamilton, T. J. Parker, S. R. P. Smith, D. R. Tilley, C. T. Foxon, D. Hilton, and K. Moore, Phys. Rev. B **46**, 2375 (1992).

[30]M. P. Chamberlain, M. Cardona, and B. K. Ridley, Phys. Rev. B **48**, 14 356 (1993).
[31]F. Bechstedt, H. Gerecke, and H. Grille, Phys. Rev. B **47**, 13 540 (1993).
[32]S. Baroni, S. de Gironcoli, and P. Giannozzi, Phys. Rev. Lett. **65**, 84 (1990).
[33]P. Giannozzi, S. de Gironcoli, P. Pavone, and S. Baroni, Phys. Rev. B **43**, 7238 (1991).
[34]G. S. Spencer, J. Grant, R. Gray, J. Zolman, and J. Menéndez, Phys. Rev. B **49**, 5761 (1994).
[35]J. Wagner, A. Fischer, W. Braun, and K. Ploog, Phys. Rev. B **49**, 7295 (1994).
[36]G. S. Spencer, A. C. Ho, J. Menéndez, R. Droopad, H. Fathollanejad, and G. N. Maracas, Phys. Rev. B **50**, 14 125 (1994).
[37]S. Baroni, P. Giannozzi, and E. Molinari, Phys. Rev. B **41**, 3870 (1990).
[38]Y. C. Chang, S. F. Ren, and H. Chu, Superlatt. Microstruct. **9**, 383 (1991).
[39]R. Enderlein, D. Suisky, and J. Röseler, Phys. Status Solidi B **165**, 9 (1991).
[40]S. F. Ren, Y. C. Chang, and H. Chu, Phys. Rev. B **47**, 1489 (1993).
[41]For reviews, see M. V. Klein, IEEE J. Quantum Electron **QE-22**, 1760 (1986); B. Jusserand and M. Cardona, in *Light Scattering in Solids V,* edited by M. Cardona and G. Güntherodt (Springer, Berlin, 1989), p. 49; J. Menédez, J. Lumin. **44**, 285 (1989).
[42]S. F. Ren, H. Chu, and Y. C. Chang, Phys. Rev. Lett. **59**, 1841 (1987).
[43]A. K. Sood, J. Menéndez, M. Cardona, and K. Ploog, Phys. Rev. Lett. **54**, 2115 (1985).
[44]For a detailed deviation of this model and supercell treatment, see G. S. Spencer, Ph.D. dissertation, Arizona State University, 1994.
[45]S. F. Ren, H. Chu, and Y. C. Chang, Phys. Rev. B **37**, 8899 (1988).
[46]K. Kunc, M. Balkanski, and M. A. Nusimovici, Phys. Rev. B **12**, 4346 (1975).
[47]*Grain Boundary Structure and Properties,* edited by G. A. Chadwick and D. A. Smith (Academic, London, 1975); *Adsorption on Metal Surfaces,* edited by J. Bénard (Elsevier, Amsterdam, 1983).
[48]J. J. Harris, D. E. Ashenford, C. T. Foxon, P. J. Dobson, and B. A. Joyce, Appl. Phys. **33**, 87 (1984).
[49]H. Jorke, Surf. Sci. **193**, 569 (1988).
[50]W. X. Ni, J. Knall, M. A. Hasan, G. V. Hansson, J. E. Sundgren, S. A. Barnett, L. C. Markert, and J. E. Greene, Phys. Rev. B **40**, 10 449 (1989).
[51]Polarizabilities were calculated as in R. Alben, J. E. Smith, Jr., M. H. Brodsky, and D. Weaire, Phys. Rev. Lett. **30**, 1141 (1973). Each polarizability was given equal weight.
[52]Varian Associates, Inc., Santa Clara, CA 95054.
[53]A. K. Sood, J. Menéndez, M. Cardona, and K. Ploog, Phys. Rev. Lett. **54**, 2111 (1985).
[54]S. B. Zhang, M. S. Hybertsen, M. L. Cohen, S. G. Louie, and D. Tomanek, Phys. Rev. Lett. **63**, 1495 (1989).
[55]S. B. Zhang, M. L. Cohen, and S. G. Louie, Phys. Rev. B **43**, 9951 (1991).
[56]D. E. Aspnes, S. M. Kelso, R. A. Logan, and R. Bhat, J. Appl. Phys. **60**, 754 (1986).
[57]The frequency shift due to the lattice constant mismatch strain was calculated as in J. Menéndez, K. Sinha, H. Höchst, and M. A. Engelhardt, Appl. Phys. Lett. **57**, 380 (1990). The uniaxial stress phonon deformation potentials used are those of GaAs [P. Wickboldt, E. Anastassakis, R. Sauer, and M. Cardona, Phys. Rev. B **35**, 1362 (1987)], following the justification of Ref. 36. The model Grüneisen parameter for AlAs used is that of Ref. 36.
[58]B. Jusserand, D. Paquet, and A. Regreny, Superlatt. Microstruct. **1**, 61 (1985).
[59]H. Morkoç, T. J. Drummond, and R. Fischer, J. Electrochem. Soc. **129**, 824 (1982).
[60]R. M. Martin, Phys. Rev. B **10**, 2620 (1974).
[61]A. J. Shields, M. Cardona, and K. Eberl, Phys. Rev. Lett. **72**, 412 (1994).